Physica B 405 (2010) 649–654

Contents lists available at ScienceDirect

Physica B

journal homepage: www.elsevier.com/locate/physb

Preparation and characterization of lithium manganese oxide cubic spinel $Li_{1.03}Mn_{1.97}O_4$ doped with Mg and Fe

Priti Singh [a], Anjan Sil [b,*], Mala Nath [a], Subrata Ray [b]

[a] Department of Chemistry, Indian Institute of Technology Roorkee, Roorkee 247667, India
[b] Department of Metallurgical and Materials Engineering, Indian Institute of Technology Roorkee, Roorkee 247667, India

ARTICLE INFO

Article history:
Received 13 June 2009
Received in revised form
18 August 2009
Accepted 22 September 2009

PACS:
82.45.Xy
81.20.Fw
61.05.C
61.72.y

Keywords:
Ceramics in electrochemistry
Sol–gel processing
X-ray diffraction and scattering
Microstructure

ABSTRACT

Spinel powders of $Li_{1.03}Mn_{1.97}O_4$, $Li_{1.03}[Mg_xMn_{1.97-x}]O_4$, $Li_{1.03}[Fe_yMn_{1.97-y}]O_4$ and $Li_{1.03}[Mg_xFe_yMn_{1.97-x-y}]O_4$ systems were synthesized by sol–gel technique using lithium acetate, manganese acetate, magnesium acetate, iron nitrate and citric acid as the starting materials. The effect of Mg and Fe substitutions on the structure and surface morphology of spinel $Li_{1.03}Mn_{1.97}O_4$ has been examined by X-ray diffraction (XRD), Field emission scanning electron microscopy (FE-SEM) and Infrared spectroscopy (IR). Electrochemical characteristics such as the cyclic performance was also investigated. The materials for all the compositions exhibit a phase pure cubic spinel structure as evident from the XRD analyses. The crystallinity and average particle size of the material increases by doping with Fe and Mg. The particles of doped samples have truncated octahedral shape. The discharge capacity of $Li_{1.03}Mn_{1.97}O_4$ is 126 mAh/g. The doping increases cyclability; however, the discharge capacity reduces.

1. Introduction

Cubic spinel lithium manganese oxide ($LiMn_2O_4$) is an attractive material for cathode over $LiCoO_2$, $LiNiO_2$, and $LiCo_{1/3}Ni_{1/3}Mn_{1/3}O_2$ in terms of lower cost and lower toxicity [1–3]. The main problem with $LiMn_2O_4$ is the capacity fading upon cycling which may become very severe at elevated temperature ($>40\,^{\circ}C$) [4]. In the spinel $LiMn_2O_4$, Li occupy tetrahedral 8a sites, Mn ions octahedral 16d sites, and O anions are arranged in 32e cubic close packing. Tetrahedral sites (8a) share faces with vacant octahedral sites (16c), so that the 16d sites form three dimensional vacant channels. In $LiMn_2O_4$, Mn exists in Mn^{4+} ($t_{2g}^3e_g^0$) and Mn^{3+} ($t_{2g}^3e_g^1$) states. Mn^{3+} ions are Jahn Teller active. The capacity fading that occurs in $LiMn_2O_4$ is due the structural transformation from cubic to tetragonal with cycling. This structural transformation is due to the $Mn^{3+}(3d^4)$ [5]. Capacity fading is also caused due to lattice instability [6], manganese dissolution [7], oxidation of the electrolyte [8], formation of oxygen rich spinel and particle disruption [9]. Several studies have been conducted to enhance the cyclic performance of $LiMn_2O_4$ at room temperature by the partial substitution of Mn in $LiMn_2O_4$ with other a trivalent cations (e.g. Fe, Al, Ni, Cr) or divalent cations (e.g. Zn, Mg), because it reduces the Mn^{3+} content and stabilizes the cubic structure of the spinel [10–13].

In recent years spinel lithium manganese oxide and the substituted compounds have been prepared mainly by solid-state reactions, pechini process, hydrothermal route and emulsion method [14–16]. However, these processes have several disadvantages, such as in homogeneity, irregular morphology, larger particle size, and requirement of long heating time followed by several regrinding. Sol–gel processing has proved to be a potential method for the synthesis of such high performance functional materials. This method has several advantages such as good control on powder stoichiometry, lower calcination temperature, relatively low processing time and production of submicron sized particle with narrow particle size distribution. It is well known that the electrochemical performance of the electrode is strongly affected by the powder properties, such as the particle morphology, the specific surface area and the powder crystallinity.

In the present study, the base compound considered is $Li_{1.03}Mn_{1.97}O_4$ due to its more lithium content while retaining in the same structure as $LiMn_2O_4$. Single and double doping by Mg and Fe in the base structure have been considered and the following lithium manganese spinel systems viz. $Li_{1.03}Mg_xMn_{1.97-x}O_4$, $Li_{1.03}Fe_yMn_{1.97-y}O_4$ and $Li_{1.03}Mg_xFe_yMn_{1.97-x-y}O_4$ were prepared to

* Corresponding author. Tel.: +91 1332 285073; fax: +91 1332 285243, 91 1332 273560.
E-mail addresses: asil1fmt@iitr.ernet.in, anj_sil@yahoo.co.uk (A. Sil).

0921-4526/$ - see front matter © 2009 Elsevier B.V. All rights reserved.
doi:10.1016/j.physb.2009.09.081

present a comparative study of the physical and electrochemical characteristics of all these systems. The compounds were synthesized by sol–gel process using citric acid as a chelating agent. To the best of authors' knowledge that synthesis of $Li_{1.03}Mn_{1.97}O_4$ spinel cathode materials codoped with Fe and Mg have not been reported, so far. The physical characterizations and the electrochemical behavior of the materials synthesized have been reported in this article.

2. Experimental procedure

The compound oxide powders in the following systems of $Li_{1.03}Mn_{1.97}O_4$, $Li_{1.03}Mg_xMn_{1.97-x}O_4$, $Li_{1.03}Fe_yMn_{1.97-y}O_4$ and $Li_{1.03}Mg_xFe_yMn_{1.97-x-y}O_4$ have been synthesized by sol–gel method using citric acid as a chelating agent. The stoichiometric amount of $Li(CH_3COO)\cdot 2H_2O$ (Thomas Baker, 99%), $Mn(CH_3COO)_2\cdot 4H_2O$ (Merck, 99.5%), $Mg(CH_3COO)_2\cdot 2H_2O$ (Thomas Baker, 99%) and $Fe(NO_3)_2\cdot 9H_2O$ (Qualigens, 98%) have been used as raw materials for the precursor. The ratio of metal ions to citric acid is kept nearly 1.0. The acetates and nitrate were dissolved separately in appropriate quantities of distilled water and the solutions were mixed together. Saturated aqueous solution of citric acid prepared separately was added at a control rate in the solution mixture. A clear transparent sol was formed which was converted to clear viscous gel by continuous stirring while heating at 100–120 °C. The pH of the mixed solution was adjusted to value between 6 and 7 by adding ammonium hydroxide solution. The gel formed was dried at 140 °C for 5–6 h to obtain the precursor compound oxide powder. The powder was then calcined at about 750 °C for 15 h in air. *The heating and cooling rates during calcination were maintained* 1 °C min^{-1}.

The structure and phase of the synthesized powders were determined by X-ray powder diffraction analysis using CuK_α radiation (λ = 1.54 Å), scanning over a range of 10–90° at the rate of 0.5°/min. Stripping of $CuK\alpha_2$ radiation was performed during the analysis. Structure parameters were obtained by using the Rietveld method with the X'Pert High Score Plus software. The reproducibility of the (a) background parameters, (b) scale factors, (c) instrumental effects (particle size broadening and strain broadening), (d) structural parameters, (e) profile parameters, and (f) phase analysis were considered for structural refinement process until the results converged into minimum values. Instrumental broadening *U*, *V* and *W* were determined from the Rietveld refinement of XRD pattern of silicon powder sample (a standard for quantitative analysis in XRD), and the results were used in the refinement of all patterns. *The lattice parameters were obtained from the Rietveld analysis*.

The morphology of the powders was observed by field emission scanning electron microscope (FEI QUANTA 200 F). Infrared spectra of the samples were recorded in a Thermonicolet (Anexus) at room temperature on a FTIR 1600 series. The sample powder was ground along with potassium bromide (Aldrich, 99.9%) and the powder mixture was pressed in a die at a load of 10 Ton.

Electrode preparation, cell construction, and sealing were carried out in an Ar gas filled glove box (MBRAUN-MB 200G) having oxygen concentration of <1 ppm. Positive electrode was made by mixing 70% active material, 15% polyvinylidene difluoride (PVDF) binder and 15% acetylene black in N-methyl-2-pyrrolidine (NMP) solvent. Mixed slurry diluted in NMP was uniformly spread by using doctor-blade on one side of aluminium foil of known weight and dried at 140 °C for 24 h in a vacuum oven. The foil with dried spread on it was rolled and dried further at 140 °C for 2 h. The mass of the cathode active material was determined from the difference in weight between aluminium foil and the foil with dried powder spread. The electrochemical measurements were carried out by constructing a teflon cell with a small piece of lithium foil as negative electrode. The electrolyte used was 1 M $LiPF_6$ dissolved in a 1:1 vol% mixture of ethylene carbonate and diethyl carbonate. Polypropylene films were used as separator. The cell was tested at a constant current of 100 μA between 3.0 and 4.3 V at 20 °C by using computer controlled system.

3. Result and discussion

3.1. X-ray diffraction analysis

Rietveld refinement of the X-ray diffraction pattern of the powder samples with compositions $Li_{1.03}Mn_{1.97}O_4$, $Li_{1.03}Fe_{0.2}Mn_{1.77}O_4$, $Li_{1.03}Mg_{0.2}Mn_{1.77}O_4$ and $Li_{1.03}Mg_{0.1}Fe_{0.1}Mn_{1.77}O_4$ have been performed using X'Pert HighScore Plus software. Fig. 1 shows refined patterns of the calcined powders of the compounds mentioned above. Refinement parameters such as R_{exp} (expected), R_p (profile), R_{wp} (weighted profile) and GOF (goodness of fit) are listed in Table 1. Atomic positions and site occupancy factors have

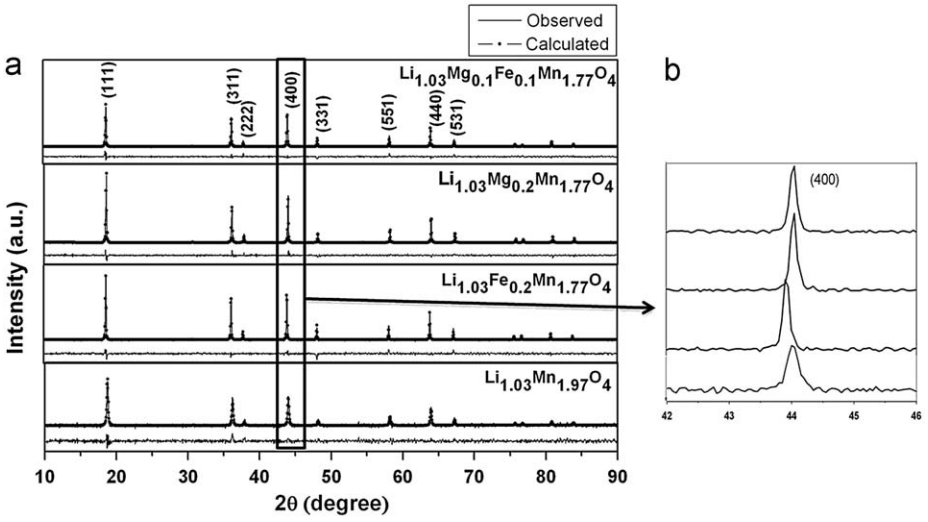

Fig. 1. (a) Rietveld refinement plots of $Li_{1.03}Mn_{1.97}O_4$, $Li_{1.03}Fe_{0.2}Mn_{1.77}O_4$, $Li_{1.03}Mg_{0.2}Mn_{1.77}O_4$ and $Li_{1.03}Mg_{0.1}Fe_{0.1}Mn_{1.77}O_4$. Observed data points are shown as straight line (-) and calculated data points by small circle (○) and difference plots are shown at bottom (b) enlarged view of (4 0 0) peaks.

Table 1
Reitveld refinement results.

Composition	Lattice parameter (Å)	R_{exp} (%)	R_{wp} (%)	R_p (%)	GOF	R_{Bragg} (%)
$Li_{1.03}Mn_{1.97}O_4$	8.2400	7.820	6.665	5.233	0.726	2.852
$Li_{1.03}Fe_{0.2}Mn_{1.77}O_4$	8.241	5.311	4.685	3.536	0.778	3.785
$Li_{1.03}Mg_{0.1}Fe_{0.1}Mn_{1.77}O_4$	8.2395	5.119	4.881	3.634	0.909	3.200
$Li_{1.03}Mg_{0.2}Mn_{1.77}O_4$	8.2203	5.143	4.213	3.230	0.671	1.480

Table 2
Site occupancy of various ions in $Li_{1.03}Mn_{1.97}O_4$, $Li_{1.03}Fe_{0.2}Mn_{1.77}O_4$, $Li_{1.03}Mg_{0.2}Mn_{1.77}O_4$ and $Li_{1.03}Mg_{0.1}Fe_{0.1}Mn_{1.77}O_4$.

Phase	Atom	Wyckoff positions	Site occupancy factor (s.o.f)	Coordinates		
				x	*y*	*z*
$Li_{1.03}Mn_{1.97}O_4$	Li1	8a	1.0000	0.1250	0.1250	0.1250
	Li2	16d	0.015	0.5000	0.5000	0.5000
	Mn	16d	0.985	0.5000	0.5000	0.5000
	O	32e	1.0000	0.2560	0.2560	0.2560
$Li_{1.03}Fe_{0.2}Mn_{1.77}O_4$	Li1	8a	1.0000	0.1250	0.1250	0.1250
	Li2	16d	0.015	0.5000	0.5000	0.5000
	Mn	16d	0.885	0.5000	0.5000	0.5000
	Fe	16d	0.1000	0.5000	0.5000	0.5000
	O1	32e	1.0000	0.2570	0.2570	0.2570
$Li_{1.03}Mg_{0.2}Mn_{1.77}O_4$	Li1	8a	1.000	0.1250	0.1250	0.1250
	Li2	16d	0.015	0.5000	0.5000	0.5000
	Mn	16d	0.885	0.5000	0.5000	0.5000
	Mg	16d	0.100	0.5000	0.5000	0.5000
	O1	32e	1.000	0.2500	0.2500	0.2500
$Li_{1.03}Mg_{0.1}Fe_{0.1}Mn_{1.77}O_4$	Li1	8a	1.0000	0.1250	0.1250	0.1250
	Li2	16d	0.015	0.5000	0.5000	0.5000
	Mn	16d	0.885	0.5000	0.5000	0.5000
	Mg	16d	0.050	0.5000	0.5000	0.5000
	Fe	16d	0.050	0.5000	0.5000	0.5000
	O1	32e	1.000	0.2560	0.2560	0.2560

Table 3
FWHM and intensity of the (4 0 0) diffraction peak of various samples.

Composition	Relative intensity of the (4 0 0) diffraction peak	FWHM of the (4 0 0) peak (deg)
$Li_{1.03}Mn_{97}O_4$	55	0.2180
$Li_{1.03}Fe_{0.2}Mn_{1.77}O_4$	70	0.1115
$Li_{1.03}Mg0.2Mn_{1.77}O_4$	71	0.1064
$Li_{1.03}Mg_{0.1}Fe_{0.1}Mn_{1.77}O_4$	74	0.1023

been refined in order to minimize the difference between observed and calculated patterns. The refined structural parameters for all compositions are given in Table 2. All the compositions have single phase cubic spinel structure with space group Fd3m at room temperature. In this structure the Li ions occupy the 8a sites and Mn, substituted ions reside at the 16d sites and O ions are present at 32e sites. Ohzuku et al. suggested that the intensity of (2 2 0) peak (at 2θ=30°) increases with the increase in site occupancy of the 8a sites [17]. It can be seen from Fig. 1 that substitution of Mn with other transition metal ions such as Fe and Mg has no effect on the intensity of (2 2 0) peak. This can be attributed to the fact that the Fe and Mg does not occupy 8a site and consequently all the Fe and Mg ions have occupied the 16d octahedral sites. Lattice parameters of different compositions are given in Table 1. It can be observed from the various refined lattice parameter values that Fe and Mg have opposite effect. Lattice parameter increases with increase in Fe content, whereas the increase in Mg content reduces the lattice parameter.

The full-width at half-maximum (FWHM) of the (4 0 0) peak is an important factor to estimate the crystallinity of the $LiMn_2O_4$ spinel powder [18]. Table 3 presents the FWHM and intensity of the (4 0 0) diffraction peak of the samples in the systems of $Li_{1.03}Mn_{1.97}O_4$, $Li_{1.03}Mg_{0.2}Mn_{1.77}O_4$, $Li_{1.03}Fe_{0.2}Mn_{1.77}O_4$, and $Li_{1.03}Mg_{0.1}Fe_{0.1}Mn_{1.77}O_4$. The doped samples show smaller FWHM and a higher intensity of the (4 0 0) peak than that of $Li_{1.03}Mn_{1.97}O_4$ sample and it indicates that the $Li_{1.03}Mg_{0.2}Mn_{1.77}O_4$, $Li_{1.03}Fe_{0.2}Mn_{1.77}O_4$, and $Li_{1.03}Mg_{0.1}Fe_{0.1}Mn_{1.77}O_4$ samples have larger crystallinity. The FWHM of the peak (4 0 0) for single Mg and doubly doped (Mg and Fe both) samples is lower compared to undoped and Fe doped samples.

3.2. Morphological study

The morphology of the synthesized powders has been observed by field emission scanning electron microscopy (FE-SEM) and the micrographs are shown in Fig. 2. It is clear from Fig. 2 that the average particle size of the doped samples is slightly *larger* than that of undoped $Li_{1.03}Mn_{1.97}O_4$ sample. This can be explained due to the fact that in doped sample the growth of the particles is higher than the nucleation rate. It can be seen from Fig. 2(a) that the particles are nearly spherical in $Li_{1.03}Mn_{1.97}O_4$ compound. Particles of truncated octahedral shape have been observed for Fe and Mg doped samples. In $Li_{1.03}Mg_{0.1}Fe_{0.1}Mn_{1.77}O_4$ compound, most of the particles have well-defined truncated octahedral shape (truncation occurred on all the edges); however, some particles have octahedral shape truncated only on two edges. It shows evolution of particles shape

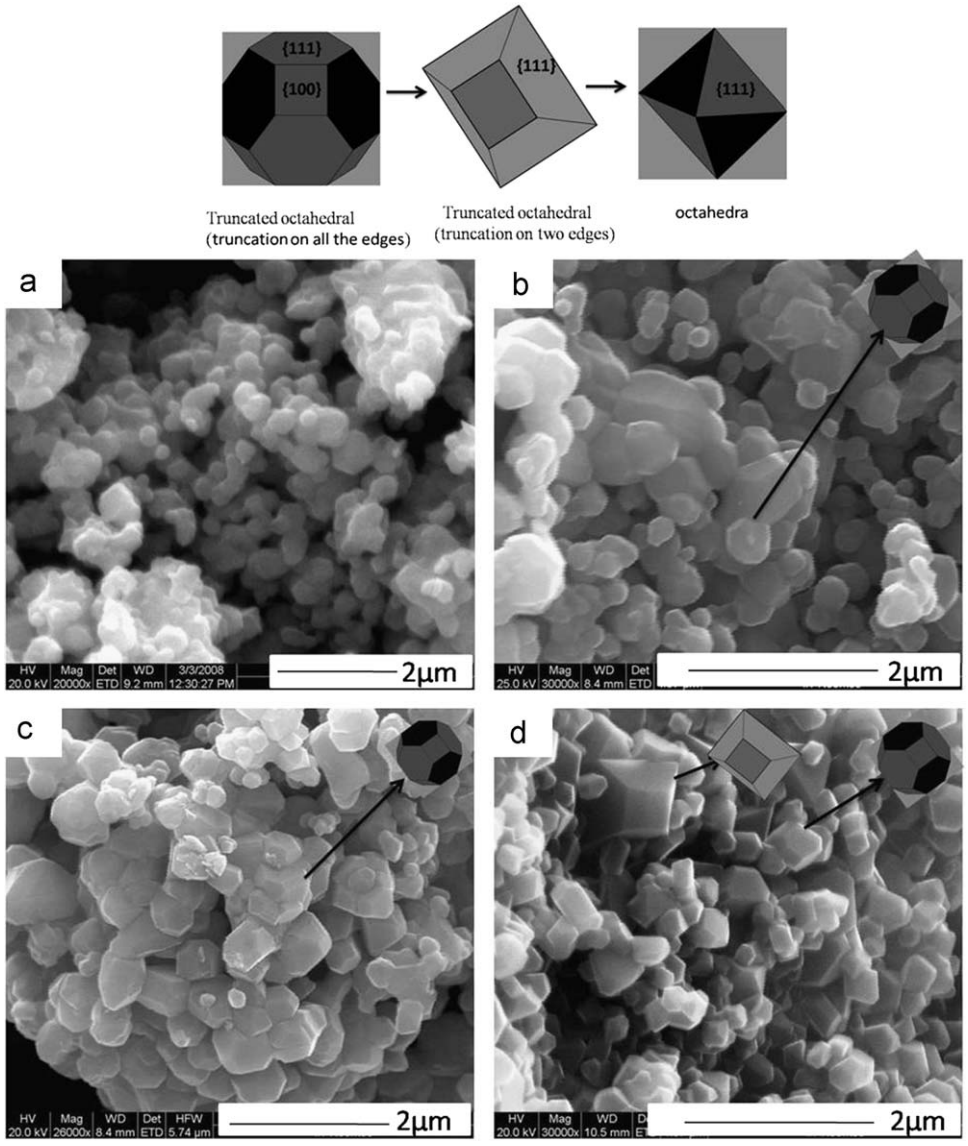

Fig. 2. FE-SEM micrographs of (a) $Li_{1.03}Mn_2O_4$, (b) $Li_{1.03}Fe_{0.2}Mn_{1.77}O_4$, (c) $Li_{1.03}Mg_{0.2}Mn_{1.77}O_4$ and (d) $Li_{1.03}Mg_{0.1}Fe_{0.1}Mn_{1.77}O_4$.

from truncated octahedral to octahedral having lower energy in case of Fe–Mg double doped compound. This is possible only if the growth rate along the {1 0 0} is much faster than that of {1 1 1} surfaces. The formation of octahedral is due to the lower energy of {1 1 1} surface. The particles in all samples are slightly in agglomerated state, as the decrease in the open surface area of the particles lowers their surface energy. Such state of particles is also beneficial for higher packing density leading to higher bulk capacity [19].

3.3. FTIR study

Fig. 3 shows the IR spectra of $Li_{1.03}Mn_{1.97}O_4$, $Li_{1.03}Fe_{0.2}Mn_{1.77}O_4$, $Li_{1.03}Mg_{0.2}Mn_{1.77}O_4$ and $Li_{1.03}Mg_{0.1}Fe_{0.1}Mn_{1.77}O_4$ compounds at room temperature. The room temperature spectrum of $Li_{1.03}Mn_{1.97}O_4$ consists mainly of two strong absorption bands at 514 and 617 cm^{-1}, which are mainly attributed to the asymmetric stretching modes of MnO_6 octahedra [20]. In case of $Li_{1.03}Fe_{0.2}Mn_{1.77}O_4$, the replacement of Mn by Fe ions results in a red shift of the high wavenumber band, which is due to the higher atomic mass of Fe. The blue shift of the band present at higher wavenumber in $Li_{1.03}Mg_{0.2}Mn_{1.77}O_4$ is due to the replacement of

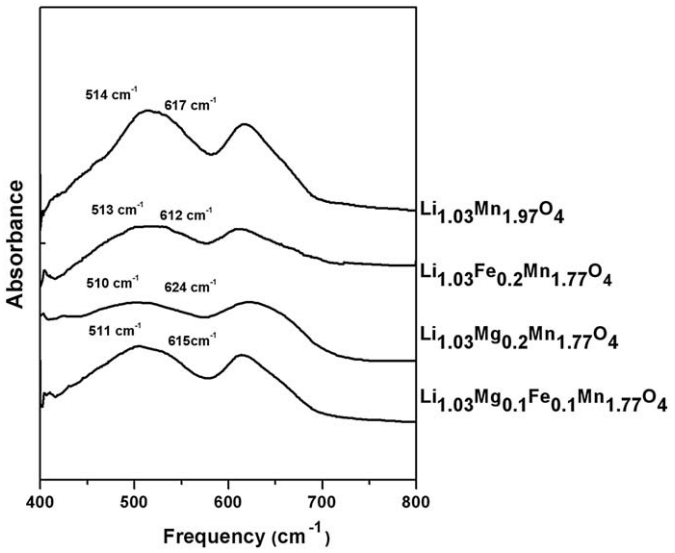

Fig. 3. IR spectra of $Li_{1.03}Mn_{1.97}O_4$, $Li_{1.03}Fe_{0.2}Mn_{1.77}O_4$, $Li_{1.03}Mg_{0.2}Mn_{1.77}O_4$ and $Li_{1.03}Mg_{0.1}Fe_{0.1}Mn_{1.77}O_4$.

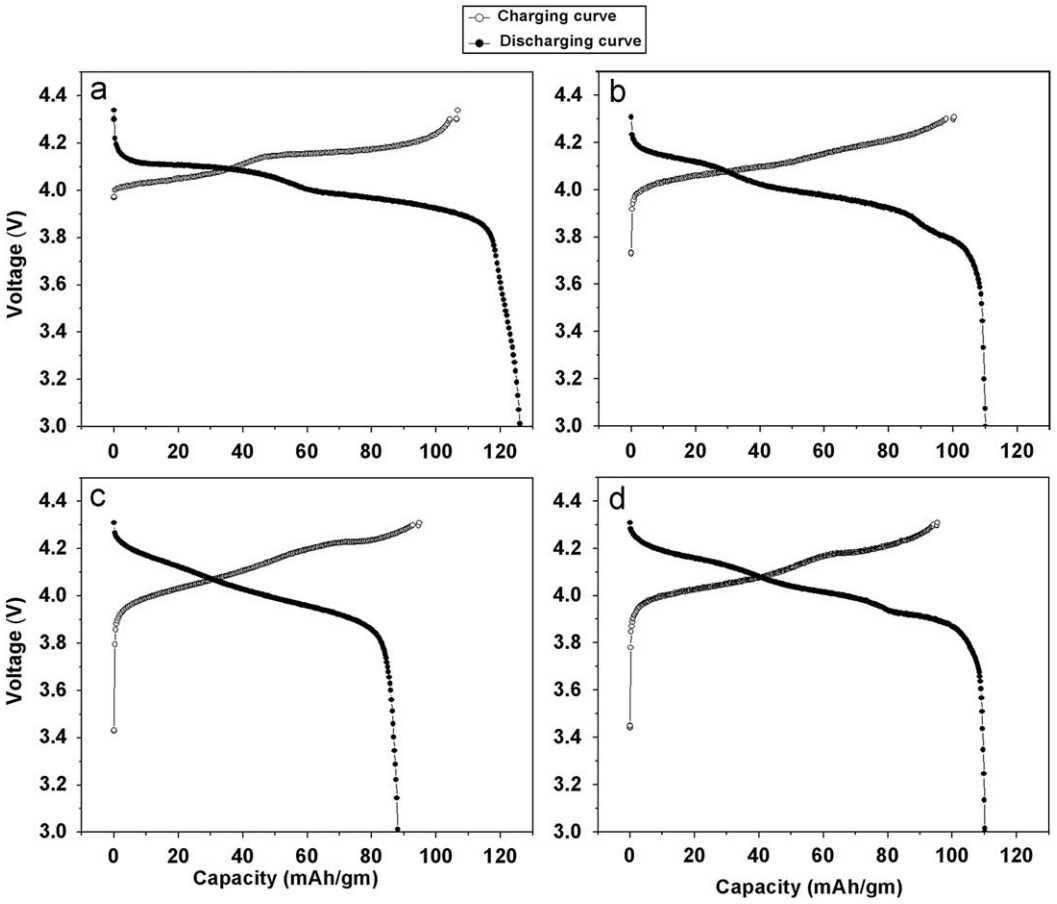

Fig. 4. First charge and discharge curves of (a) $Li_{1.03}Mn_2O_4$, (b) $Li_{1.03}Fe_{0.2}Mn_{1.77}O_4$, (c) $Li_{1.03}Mg_{0.2}Mn_{1.77}O_4$ and (d) $Li_{1.03}Mg_{0.1}Fe_{0.1}Mn_{1.77}O_4$.

the Mn ions by Mg ions, which have lower atomic mass compared to Mn. The composition $Li_{1.03}Mg_{0.1}Fe_{0.1}Mn_{1.77}O_4$ shows two frequency bands at 511 and 615 cm^{-1}, which represent the simultaneous effect of Mg and Fe dopings in the material $Li_{1.03}Mn_{1.97}O_4$.

3.4. Electrochemical properties

Fig. 4 shows the charge and discharge capacity curves of $Li_{1.03}Mn_{1.97}O_4$, $Li_{1.03}Fe_{0.2}Mn_{1.77}O_4$, $Li_{1.03}Mg_{0.2}Mn_{1.77}O_4$ and $Li_{1.03}Mg_{0.1}Fe_{0.1}Mn_{1.77}O_4$ samples in a voltage range of 3–4.3 V. A voltage step at 4.1 V appears for $Li_{1.03}Mn_{1.97}O_4$ as shown in Fig. 4. Ohzuku et al. [21], however, observed the voltage step at 4.11 V in $LiMn_2O_4$ and attributed this to the transition from two cubic phases to a single cubic phase. The voltage step reduces due to doping with Fe and Mg, implying the cubic phase stability. The Mg-substituted compound maintains single phase during intercalation and deintercalation of lithium without a subtle voltage change at 4.1 V. It can be seen that the initial discharge capacity of $Li_{1.03}Mn_{1.97}O_4$ is 126 mAh/g which is higher than that of Fe and Mg doped samples. Decrease in capacity of $Li_{1.03}Fe_{0.2}Mn_{1.77}O_4$, $Li_{1.03}Mg_{0.2}Mn_{1.77}O_4$ and $Li_{1.03}Mg_{0.1}Fe_{0.1}Mn_{1.77}O_4$ is due to decrease in the Li content which can be extracted. The removal of lithium from the spinel is accompanied by oxidation of Mn^{3+} to Mn^{4+}.

The variation of discharge capacities in $Li/Li_{1.03}Mn_{1.97}O_4$, $Li/Li_{1.03}Fe_{0.2}Mn_{1.77}O_4$, $Li/Li_{1.03}Mg_{0.2}Mn_{1.77}O_4$ and $Li/Li_{1.03}Mg_{0.1}Fe_{0.1}Mn_{1.77}O_4$ with increasing number of charge–discharge cycles is shown in Fig. 5. It can be seen from the figure that the first discharge capacity of $Li_{1.03}Mn_{1.97}O_4$ is 126 mAh/g, which reduces to 118 mAh/g after 10 cycles. However, first discharge capacity of $Li_{1.03}Fe_{0.2}Mn_{1.77}O_4$ is 110 mAh/g which reduces to 109 mAh/g after 10 cycles. The discharge capacity of $Li_{1.03}Mg_{0.2}Mn_{1.77}O_4$ is lower, the first cycle shows 88 mAh/g, which reduces to 87 mAh/g. Higher capacity retention has been found with

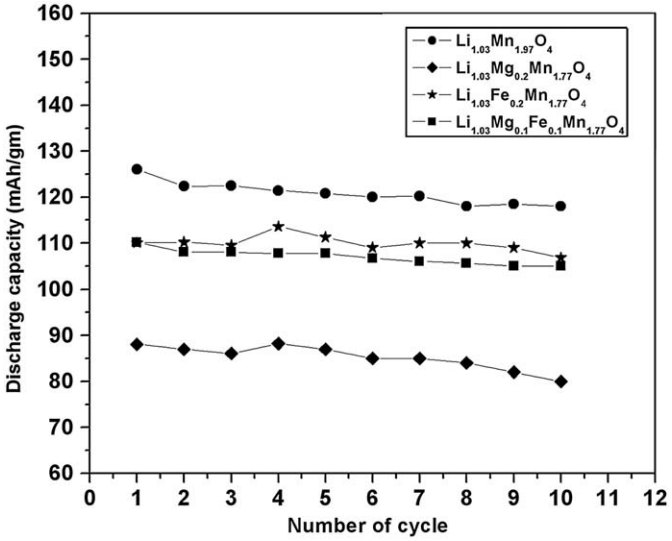

Fig. 5. Discharge capacity vs. cycle number for the cell $Li/Li_{1.03}Mn_{1.97}O_4$, $Li/Li_{1.03}Fe_{0.2}Mn_{1.77}O_4$, $Li_{1.03}Mg_{0.2}Mn_{1.77}O_4$ and $Li/Li_{1.03}Mg_{0.1}Fe_{0.1}Mn_{1.77}O_4$ between 3.0 and 4.3 V at room temperature.

$Li_{1.03}Mg_{0.1}Fe_{0.1}Mn_{1.77}O_4$, the first discharge capacity is 110 mAh/g which reduces to 107 mAh/g after 10 cycles. The lower discharge capacity of doped sample with $Li_{1.03}Mn_{1.97}O_4$ is due to the substitution of Fe^{3+}, Mg^{2+} into the Mn^{3+} site resulting in oxidation of Mn^{3+} to Mn^{4+}, which increases the stability of cubic spinel, reported also by Li et al. [22].

4. Conclusions

Following conclusions can be drawn from the present study:

1. XRD analyses show that the materials of all the compositions studied have a phase pure cubic spinel structure having Fd3m space group. Lattice parameter of the unit cell increases with Fe doping and decreases with Mg doping.
2. $Li_{1.03}Mg_{0.1}Fe_{0.1}Mn_{1.77}O_4$ samples have larger crystallinity than other samples. The FWHM of the peak (4 0 0) for single Mg and doubly doped (Mg and Fe both) samples is lower compared to undoped and Fe doped samples.
3. Average particle sizes in the Fe doped and Mg doped samples are slightly greater than that of undoped $Li_{1.03}Mn_{1.97}O_4$ sample. The particles in all the samples are slightly in agglomerated state. The particles having truncated octahedral shape have been observed for Fe and Mg doped samples.
4. The discharge capacity of $Li_{1.03}Mn_{1.97}O_4$ is about 126 mAh/g. The voltage step corresponding to the two cubic phase transition reduces in Fe and Mg doped samples.
5. Doped compounds show better capacity retention than undoped compound.

References

[1] G.G. Amatucci, J.M. Tarascon, L.C. Klein, CoO_2, the end member of the $LiCoO_2$ solid solution, J. Electrochem. Soc. 143 (3) (1996) 1114.
[2] S.P. Sheu, I.C. Shih, C.Y. Yao, J.M. Chen, W.M. Hurng, Studies of $LiNiO_2$ in lithium ion batteries, J. Power Sources 68 (1997) 558.
[3] N. Yabuuchi, T. Ohzuku, Electrochemical behaviors of $LiCo_{1/3}Ni_{1/3}Mn_{1/3}O_2$ in lithium batteries at elevated temperatures, J. Power Sources 146 (2005) 636.
[4] R.J. Gummow, A. de Kock, M.M. Thackeray, Improved capacity retention in rechargeable 4 V lithium/lithium manganese oxide (spinel) cells, J. Solid State Ionics 69 (1994) 59.
[5] J.D. Dunitz, L.E. Orgel, Electronic properties of transition metal oxide—I distortion from cubic symmetry, J. Phys. Chem. Solids 3 (1957) 20.
[6] A. Yamada, Lattice instability in $Li(Li_xMn_{2-x})O_4$, J. Solid State Chem. 122 (1996) 160.
[7] D.H. Jang, J.Y. Shin, S.M. Oh, Dissolution of spinel oxides and capacity losses in 4 V $Li/Li_xMn_2O_4$ cells, J. Electrochem. Soc. 143 (1996) 2204.
[8] Y. Gao, J.R. dahnDahn, Correlation between the growth of the 3.3 V discharge plateau and capacity fading in $Li_{1+x}Mn_{2-x}O_4$ materials, Solid State Ionics 84 (1996) 33.
[9] S.-T. Myung, H.-T. Chung, S. Komaba, N. Kumagai, H.-B. Gu, Capacity fading of $LiMn_2O_4$ electrode synthesized by the emulsion drying method, J. Power Sources 90 (2000) 103.
[10] L. Guohua, H. Ikuto, T. Uchida, M. Wakihara, The spinel phases $LiM_yMn_{2-y}O_4$ (M=Co, Cr, Ni) as the cathode for rechargeable lithium batteries, J. Electrochem. Soc. 143 (1996) 178.
[11] Q. Feng, H. Kanoh, Y. Miyai, K. Ooi, Li^+ extraction/insertion reactions with $LiZn_{0.5}Mn_{l.5}O_4$ spinel in the aqueous phase, J. Chem. Mater. 7 (1995) 379.
[12] T. Nakamura, H. Demidzu, Y. Yamada, Synthesis and magnetic study on Mg^{2+}-substituted Li–Mn spinel oxides, J. Phys. Chem. Solids 69 (2008) 2349.
[13] O. Tanaike, M. Kodama, H. Hatori, High rate capability of the Mg-doped Li–Mn–O spinel prepared via coprecipitated precursor, J. Power Sources 168 (2007) 282.
[14] S.-h. Wu, H.-l. Chen, The effects of heat-treatment temperature on the retention capacities of spinels prepared by the Pechini process, J. Power Sources 119–121 (2003) 134.
[15] G. Li, A. Yamada, Y. Fukushima, K. Yamaura, T. Saito, T. Endo, H. Azuma, K. Sekai, Y. Nishi, Phase segregation of $Li_xMn_2O_4$ ($0.6 < x < 1$) in non-equilibrium reduction processes, Solid State Ionics 130 (2000) 221.
[16] B.J. Hwang, R. Santhanam, D.G. Liu, Characterization of nanoparticles of $LiMn_2O_4$ synthesized by citric acid sol–gel method, J. Power Sources 97 (2001) 443.
[17] T. Ohzuku, K. Ariyoshi, S. Takeda, Y. Sakai, Synthesis and characterization of 5 V insertion material of $Li[FeyMn_{2-y}]O_4$ for lithium-ion batteries, J. Electrochimica Acta 46 (2001) 2327.
[18] D.S. Ahn, M.Y. Song, Variations of the electrochemical properties of $LiMn_2O_4$ with synthesis conditions, J. Electrochem. Soc. 147 (3) (2000) 874.
[19] R. Thirunakaran, K.-T. Kim, Y.M. Kang, J. Young-Lee, Cr^{3+} modified $LiMn_2O_4$ spinel intercalation cathodes through oxalic acid assisted sol–gel method for lithium rechargeable batteries, J. Materials Research Bulletin 40 (2005) 177.
[20] C.M. Julien, M.A. Camacho-Lopez, Lattice vibrations of materials for lithium rechargeable batteries II. Lithium extraction-insertion in spinel structure, J. Mater. Sci. Eng. B 108 (2004) 179.
[21] T. Ohzuku, M. Kitagawa, T. Hirai, Electrochemistry of manganese dioxide in lithium nonaqueous cell III. X-ray diffractional study on the reduction of spinel-related manganese dioxide, J. Electrochem. Soc. 137 (3) (1990) 769.
[22] L. Guohua, H. Ikuta, M. Uchida, M. Wakihara, The spinel phases $LiM_yMn_{2-y}O_4$ (M=Co, Cr, Ni) as the cathode for rechargeable lithium batteries, J. Electrochem. Soc. 143 (1996) 178.